NGA-West2 models for ground-motion directionality

Shrey K. Shahi,[a], and Jack W. Baker[b] M.EERI

The NGA-West2 research program, coordinated by the Pacific Earthquake Engineering Research Center (PEER), is a major effort to produce refined models for predicting ground-motion response spectra. This study presents new models for ground-motion directionality developed as part of that project. Using a database of recorded ground motions, empirical models have been developed for a variety of quantities related to direction-dependent spectra. A model is proposed for the maximum spectral acceleration observed in any orientation of horizontal ground-motion shaking ($Sa_{RotD100}$), which is formulated as a multiplicative factor to be coupled with the NGA-West2 models that predict the median spectral accelerations over all orientations (Sa_{RotD50}). Models are also proposed for the distribution of orientations of the $Sa_{RotD100}$ value relative to the fault and the relationship between $Sa_{RotD100}$ orientations at differing periods. Discussion is provided as to how these results can be applied to perform seismic hazard analysis and compute realistic target spectra conditioned on different parameters.

INTRODUCTION

Structures in seismically active regions are generally designed considering ground motion in the horizontal plane. The spectral acceleration (*Sa*) value of a single component of a ground motion is defined as the maximum response of a single degree of freedom system with a specified period and damping (5% damping is assumed below, and *Sa* here refers to pseudo spectral acceleration). For a ground motion with shaking in multiple horizontal directions, some method is needed to combine the directionally-varying single-component *Sa* values into a single numerical value. Various methods have been proposed to compute a spectral acceleration value representative of the two-dimensional horizontal ground motion. These methods include using the geometric mean of the acceleration response spectra

[a] Virginia Tech, Blacksburg, VA 24060
[b] Stanford University, Y2E2, Stanford, CA 94305

computed using two orthogonal components of ground motion and using the median or maximum value of response spectra over all orientations at each period (Boore et al., 2006; Boore, 2010).

The NGA-West2 research program, coordinated by Pacific Earthquake Engineering Research Center (PEER), has produced models for predicting the median spectral acceleration of a ground motion when rotated over all horizontal orientations (Bozorgnia et al., 2012); this is referred as the Sa_{RotD50} value (Boore, 2010), and will be discussed further in the following section. On the other hand, some engineers believe that the maximum spectral acceleration over all orientations ($Sa_{RotD100}$) is more meaningful than Sa_{RotD50} for structural design (e.g., NEHRP, 2009). Thus, different definitions of ground-motion intensities will be used to build ground-motion models (Sa_{RotD50}) and for structural design ($Sa_{RotD100}$). The need to use a consistent spectral acceleration definition throughout the design process (e.g., Baker and Cornell, 2006; Beyer and Bommer, 2006) requires models to convert between the two definitions of *Sa*. Additionally, there is interest in whether the $Sa_{RotD100}$ is observed in random orientations or has preferential alignment in, for example, near-fault ground motions. This also has potentially important implications for structural design.

Several researchers have studied polarization or directionality of ground motions. Past studies included investigation of principal axes of the ground motion (e.g., Kubo and Penzien, 1976, 1979; Loh et al., 1982; Hong and Goda, 2010) and critical angle of incidence (e.g., Lopez and Torres, 1997; Lopez et al., 2000). In the current study we develop empirical models to be used with NGA-West2 ground-motion model predictions, by studying the ratios of Sa_{RotD50} and other Sa definitions. Other researchers have developed models for ratios of different *Sa* definitions in past (e.g., Beyer and Bommer, 2006; Watson-Lamprey and Boore, 2007; Campbell and Bozorgnia, 2007, 2008; Huang et al., 2008, 2010). Most of these studies used subsets of the NGA database (Chiou et al., 2008) and focused on the ratios involving the older $Sa_{GMRotI50}$ definition of response spectrum. In this study we use over 3000 ground motions from the expanded NGA-West2 database to build empirical models for the ratio of $Sa_{RotD100}$ to Sa_{RotD50} and the probability distribution of orientations in which the $Sa_{RotD100}$ is observed. The model predicting the ratio of $Sa_{RotD100}$ to Sa_{RotD50} is a multiplicative factor that, when used with the NGA-West2 ground-motion models, can predict the $Sa_{RotD100}$ at a site. The proposed models are compared with older models and differences are discussed.

As defined, the $Sa_{RotD100}$ values at differing periods may occur in differing orientations, so it is highly unlikely that any single orientation of a ground motion will have *Sa* value as large as the motion's $Sa_{RotD100}$ at all periods. Since dynamic response of a multi-degree-of-freedom system is related to *Sa* at a range of periods, using $Sa_{RotD100}$ as the spectrum of a single ground motion component can lead to conservative estimates of structural demand (e.g., Stewart et al., 2011). To address this, the relationship between the orientations of $Sa_{RotD100}$ at different periods is studied in detail and this information is used to compute more realistic target spectra for single ground motion components. Example computations and discussion of several alternate target spectra are included.

GROUND MOTION INTENSITY AND DIRECTIONALITY

As discussed above, spectral acceleration (*Sa*) measures the response of a single-degree-of-freedom oscillator in a single orientation and cannot completely represent a ground motion's intensity in two dimensions. Several methods have been proposed in the past to compute a scalar value of *Sa* to represent two-dimensional ground motions. Early efforts to account for the two-dimensional intensity of ground motion used the geometric mean of response spectra computed using two orthogonal components of the ground motion (sometimes referred as Sa_{GM}). Generally the two orientations in which the ground motion was recorded ("as-recorded orientations"), or the fault-normal and parallel orientations, are used for computing Sa_{GM}. Using the as-recorded orientations of the ground motion makes the ground-motion intensity dependent on the arbitrary orientation of the recording instrument, though the practical effect on *Sa* is often minor (e.g., Beyer and Bommer, 2006). The fault-normal and parallel orientations are important for near-fault sites, as near-fault effects are generally observed in these orientations (directivity in fault-normal, fling in fault-parallel for strike-slip earthquakes), but these orientations have no special significance for sites located far from the fault.

To remove the dependence of *Sa* on recording orientations, Boore et al. (2006) introduced $Sa_{GMRotDnn}$ and $Sa_{GMRotInn}$, which are orientation-independent definitions of ground-motion intensity. $Sa_{GMRotDnn}$ is defined as the nn^{th} percentile of the geometric means of the response spectra from all orthogonal components of the ground motion at a specified period. The $Sa_{GMRotDnn}$ spectrum uses the geometric means from different orientations at different periods and does not represent any particular observation of two components of the ground motion. $Sa_{GMRotInn}$ addresses this problem by computing the geometric mean response

spectrum at the specific orientation with a spectrum closest to the $Sa_{GMRotDnn}$ spectrum across a range of periods. This definition thus uses the geometric mean spectrum of two specific ground motion components that were observed at the site. The 2008 NGA ground-motion models were developed to predict $Sa_{GMRotI50}$ (Abrahamson et al., 2008).

Though the $Sa_{GMRotInn}$ spectrum captures information from multiple orientations and is orientation and period independent, it is difficult to compute. Boore (2010) proposed new spectral definitions, called Sa_{RotDnn} and Sa_{RotInn}. Sa_{RotDnn} is defined as the nn^{th} percentile of the spectral acceleration at each period over all orientations. Like $Sa_{GMRotDnn}$, the nn^{th} percentile spectral acceleration at each period may occur in different orientations. Sa_{RotInn} addresses this by computing the spectral acceleration in the orientation most representative of the Sa_{RotDnn} spectrum. Since maximum intensity at each period may occur in different orientations and Sa_{RotInn} spectrum uses a single orientation of the ground motion, the Sa_{RotI50} spectrum can be greater than the $Sa_{RotI100}$ spectrum at some periods (Boore, 2010). This is considered a shortcoming of the Sa_{RotInn} definition. Due to its simple and orientation-independent definition, Sa_{RotDnn} has recently become popular. The NGA-West2 project ground-motion models predict Sa_{RotD50} values.

When a single response spectrum is used to represent two-dimensional ground-motion shaking, there is loss of information regarding how the spectrum varies with orientation. Different definitions of ground-motion intensity capture different pieces of this information and thus may be appropriate for different tasks. If the ground motion has an approximately equal response spectrum in all orientations at a given period, we term it unpolarized. An example unpolarized case is illustrated in Figure 1a, and the ratio of $Sa_{RotD100}$ to Sa_{RotD50} is close to 1. However, if the ground motion is strongly polarized, as illustrated in Figure 1b, the various definitions of Sa will differ significantly in numerical value. In this case, the ratio of $Sa_{RotD100}$ to Sa_{RotD50} can be shown to equal $\sqrt{2} = 1.414$. *Sa* values for any ground motion will lie between these two extreme cases, so the $Sa_{RotD100}$ to Sa_{RotD50} ratio will thus lie between 1 and 1.414. The polarization of ground motion, also referred as directionality of ground motion, causes this discrepancy among different definitions of response spectra. Thus, in this study the models used to convert between different spectral acceleration definitions are referred to as directionality models.

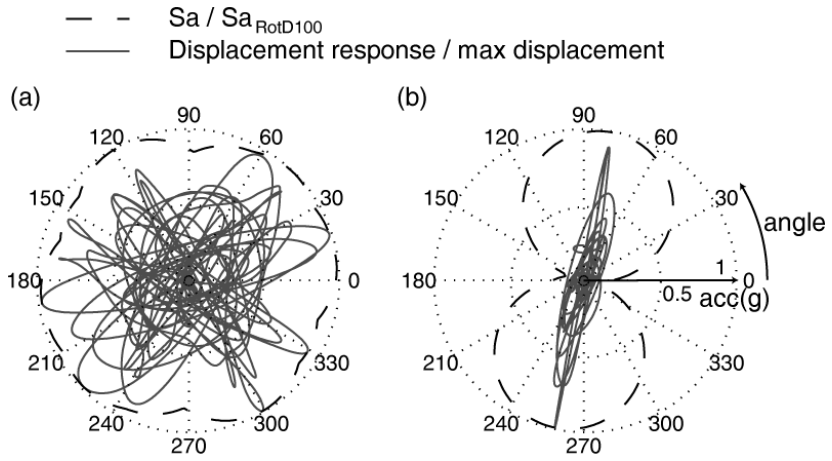

Figure 1. Normalized displacement response trace of a single-degree-of freedom oscillator with $T = 1$ second, and normalized 1 second spectral acceleration in all horizontal orientations (a) when ground motion is almost unpolarized (HWA031 recording from Chi-Chi-04, 1999 earthquake) and (b) when the ground motion is strongly polarized (Gilroy Array #6 recording from Morgan Hill, 1984 earthquake).

RATIO OF $Sa_{RotD100}$ TO Sa_{RotD50}

Some engineering provisions use $Sa_{RotD100}$ for engineering design (e.g., NEHRP, 2009) while the NGA-West2 ground-motion models are being developed to predict Sa_{RotD50} intensity. Thus, models to convert between the two definitions are needed to allow the use of consistent definition of *Sa* throughout the design process.

We computed the ratio of $Sa_{RotD100}$ to Sa_{RotD50} for each ground motion in the subset of NGA-West2 database being used to develop the Abrahamson and Silva ground-motion model (Abrahamson et al., 2013). The geometric mean of these ratios can be used as a multiplicative factor to convert Sa_{RotD50} intensity to $Sa_{RotD100}$ and its logarithm as an additive factor to convert $lnSa_{RotD50}$ to $\ln Sa_{RotD100}$. As spectral accelerations are reasonably modeled as log-normally distributed (e.g., Abrahamson, 1998; Jayaram and Baker, 2008) and the ground-motion models predict the natural log of *Sa*, the geometric mean of the ratios ($e^{\mu\, ln(Sa_{RotD100}/Sa_{RotD50})}$) is a more natural estimator than the arithmetic mean, as shown in equations 1 to 3. Multiplying and dividing $Sa_{RotD100}$ by Sa_{RotD50}, and then taking logarithms of both sides,

$$Sa_{RotD100} = \frac{Sa_{RotD100}}{Sa_{RotD50}} \cdot Sa_{RotD50} \tag{1}$$

$$lnSa_{RotD100} = ln\left(\frac{Sa_{RotD100}}{Sa_{RotD50}}\right) + lnSa_{RotD50} \tag{2}$$

and then taking expectations of both sides produces

$$\mu_{lnSa_{RotD100}} = \mu_{\,ln(Sa_{RotD100}/Sa_{RotD50})} + \mu_{lnSa_{RotD50}} \quad (3)$$

Where $\mu_{(\cdot)}$ represents the expected value or mean value. The $lnSa_{RotD50}$ term can be estimated using a NGA-West2 ground-motion model (Bozorgnia et. al, 2012) which has functional form

$$lnSa_{RotD50_{ij}} = f(M, R, \dots) + \eta_i + \epsilon_{ij} \quad (4)$$

Where $f(M, R, \dots)$ represents the ground-motion model prediction of $\mu_{lnSa_{RotD50}}$, as a function of magnitude (M), distance (R) and other parameters, η_i represents the between-event residual (also known as inter-event residual) and ϵ_{ij} represents the within-event residual (intra-event residual). The subscript i refers to i^{th} earthquake event and j refers to the j^{th} recording of i^{th} event. Similarly, the $ln\left(\frac{Sa_{RotD100}}{Sa_{RotD50}}\right)$ term can be predicted independently of the ground-motion model using a simple model shown below

$$ln\left(\frac{Sa_{RotD100}}{Sa_{RotD50}}\right)_{ij} = \mu_{\,ln(Sa_{RotD100}/Sa_{RotD50})} + \eta_i' + \epsilon_{ij}' \quad (5)$$

where η_i' represents the between-event residual and ϵ_{ij}' represents the within-event residual. Mixed effects regression (e.g., Searle, 1971; Brillinger and Preisler 1985; Abrahamson and Youngs, 1992) is used to estimate the $\mu_{\,ln(Sa_{RotD100}/Sa_{RotD50})}$. Table 1 shows the estimated $\mu_{\,ln(Sa_{RotD100}/Sa_{RotD50})}$, geometric mean of $Sa_{RotD100}/Sa_{RotD50}$, along with the between-event standard deviation (τ) and within-event standard deviation (ϕ) (standard-deviation notation following Al Atik et al., 2010). The results are reported at a discrete set of periods, and coefficients at other periods can be estimated by interpolating these results. The low values of τ show that the between-event terms for $ln(Sa_{RotD100}/Sa_{RotD50})$ are close to zero, or equivalently that the event terms for $lnSa_{RotD100}$ and $lnSa_{RotD50}$ are comparable and thus cancel out. This was expected, as any amplification or deamplification of *Sa*'s due to common source effects should be shared by both Sa_{RotD50} and $Sa_{RotD100}$. Results computed using different subsets of the NGA-West2 database used to develop other ground-motion models were found to be effectively identical. Care should be taken while modeling the residuals in equation 5. Since the $Sa_{RotD100}/Sa_{RotD50}$ ratio is bounded between 1 and 1.41 by definition, modeling the residuals by Gaussian distribution may result in non-zero probabilities assigned to physically impossible values.

Table 1. Computed values of $\mu_{ln(Sa_{RotD100}/Sa_{RotD50})}$, within-event standard deviation (ϕ), between-event standard deviation (τ) and total standard deviation (σ), estimated by mixed effects regression. The values are for mean of $ln(Sa_{RotD100}/Sa_{RotD50})$ and geometric mean of $Sa_{RotD100}/Sa_{RotD50}$ and the reported standard deviations are for $ln(Sa_{RotD100}/Sa_{RotD50})$ estimates.

Period (s)	$ln\left(\frac{Sa_{RotD100}}{Sa_{RotD50}}\right)$	$\frac{Sa_{RotD100}}{Sa_{RotD50}}$	ϕ	τ	σ_{total}
0.01	0.176	1.19	0.08	0.01	0.08
0.02	0.175	1.19	0.08	0.01	0.08
0.03	0.172	1.19	0.08	0.01	0.08
0.05	0.171	1.19	0.08	0.01	0.08
0.075	0.172	1.19	0.08	0.01	0.08
0.1	0.172	1.19	0.08	0.01	0.08
0.15	0.182	1.20	0.08	0.01	0.08
0.2	0.187	1.21	0.08	0.01	0.08
0.25	0.196	1.22	0.08	0.01	0.08
0.3	0.198	1.22	0.08	0.01	0.08
0.4	0.206	1.23	0.08	0.01	0.08
0.5	0.206	1.23	0.09	0.01	0.09
0.75	0.213	1.24	0.08	0.01	0.08
1	0.216	1.24	0.08	0.01	0.08
1.5	0.217	1.24	0.08	0.01	0.08
2	0.218	1.24	0.08	0.01	0.08
3	0.221	1.25	0.08	0.01	0.08
4	0.231	1.26	0.08	0.01	0.08
5	0.235	1.26	0.08	0.02	0.08
7.5	0.251	1.28	0.08	0.02	0.08
10	0.258	1.29	0.07	0.03	0.08

COMPARISON WITH OTHER MODELS

Several researchers have computed ratios of $Sa_{RotD100}$ to $Sa_{GMRotI50}$ from recorded ground motions (e.g., Beyer and Bommer, 2006; Watson-Lamprey and Boore, 2007; Campbell and Bozorgnia, 2007, 2008; Huang et al., 2008, 2010). To compare the older ratios of $Sa_{RotD100}$ to $Sa_{GMRotI50}$ with the $Sa_{RotD100}$ to Sa_{RotD50} ratios computed in this study, we use the factors proposed by Boore (2010) to convert the proposed $Sa_{RotD100}/Sa_{RotD50}$ ratios to $Sa_{RotD100}/Sa_{GMRotI50}$ ratios. Figure 2 shows our converted $Sa_{RotD100}$ to $Sa_{GMRotI50}$ ratios, as well as previously reported ratios. Most of these models agree with each other in both the magnitude of the ratios and their trend with period. The one exception is the ratios proposed in NEHRP (2009) provisions.

The NEHRP (2009) $Sa_{RotD100}/Sa_{GMRotI50}$ ratios are based on the ratio of observed $Sa_{RotD100}$ values in recorded ground motions to the prediction of $Sa_{GMRotI50}$ by a ground-

motion model. Modeling the ratio of an observed value to a predicted value, rather than the ratio of an observed value to an observed value, has some flaws. NGA models were carefully fitted to provide an unbiased estimate of ground-motion intensity from future earthquakes (Abrahamson et al., 2008). However, the dataset used to fit the ground-motion models is not an unbiased sample of earthquakes (e.g., there are many more ground motions from the 1999 *M*=7.6 Chi-Chi, Taiwan earthquake in the NGA database compared to other earthquakes). Statistical techniques such as mixed-effects regression have been used to overcome these biases in the dataset while fitting the NGA ground-motion models. The ratios recommended by the NEHRP (2009) provisions effectively readjust the NGA ground-motion models, which removes the benefits of careful calculations that go into building a ground-motion model. For example, a particular earthquake can produce higher average ground-motion intensities than the unbiased ground-motion model estimate due to random chance (any physical effect not accounted for by the ground-motion model can be modeled as random chance). The ratios of observed $Sa_{RotD100}$ to the predicted Sa_{RotD50} for such an earthquake will be higher than the ratio of observed $Sa_{RotD100}$ to observed Sa_{RotD50}, as the first ratio will also include the random earthquake effect, which is carefully removed by the mixed effects regression used to fit ground-motion models. Modeling $Sa_{RotD100}/Sa_{RotD50}$ as the ratio of observed $Sa_{RotD100}$ to observed Sa_{RotD50}, and using the prediction from a ground-motion model as an estimate for $lnSa_{RotD50}$ as shown in equation 4 allows us to leverage the results from careful fitting of ground-motion models and gives us a better estimate of $Sa_{RotD100}$ from a future earthquake.

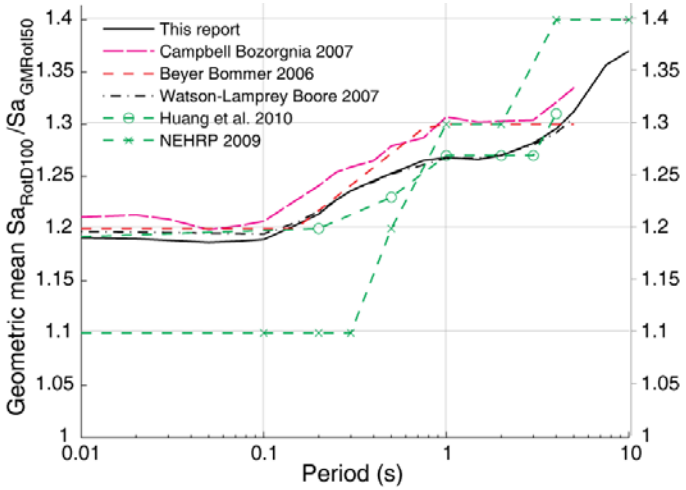

Figure 2. Comparison of various models for geometric mean $Sa_{RotD100}/Sa_{GMRotI50}$ ratios. The observed $Sa_{RotD100}$/ observed $Sa_{GMRotI50}$ratios from table 2-2 of Huang et al. (2010) are shown here.

Huang et al. (2008, 2010) reported that ground motion from Chi-Chi earthquake had a significant effect on the geometric mean of the ratio of observed $Sa_{RotD100}$ to $Sa_{GMRotI50}$

values predicted by ground-motion models, so they reported different sets of results for datasets with and without the Chi-Chi records. We found that the inclusion or exclusion of Chi-Chi records from our estimation does not change the geometric mean of observed $Sa_{RotD100}$ to observed Sa_{RotD50} significantly. This indicates that the "observed-to-observed" ratios are more numerically stable than "observed-to-predicted" ratios, which is another advantage in addition to their mathematical consistency with existing prediction models.

DEPENDENCE OF $Sa_{RotD100}/Sa_{RotD50}$ ON EARTHQUAKE PARAMETERS

Table 1 showed that the geometric mean value of $Sa_{RotD100}/Sa_{RotD50}$ depends on spectral acceleration period. We also investigated its dependence on other seismological parameters like earthquake magnitude, closest distance between source and the site and some directivity parameters. We studied the dependence of this ratio on seismological parameters and fitted several regression models using variable selection techniques like forward selection, backward elimination etc. After examining the practical and statistical significance of different models, we developed a model for $ln(Sa_{RotD100}/Sa_{RotD50})$ that was a linear function of R_{rup} (closest distance between rupture and site). Other parameters such as magnitude, directivity predictor terms, etc., had no appreciable predictive power, as documented in Shahi and Baker (2013). The linear model, shown in equation 6, contains a coefficient a_0 that varies with period and a coefficient a_1 that is constant for all periods and is equal to 1.614×10^{-4}. The coefficient a_0 is the same as the $ln(Sa_{RotD100}/Sa_{RotD50})$ values presented in table 1. This relationship was fitted using data with closest distances of less than 200km, and over 90% of the data had closest distance less than 100km, so the model should not be used for distances larger than 200km.

$$E\left[ln\left(\frac{Sa_{RotD100}}{Sa_{RotD50}}\right)\right] = a_0 - a_1 \cdot (R_{rup} - 60) \quad (6)$$

The difference between the results from using a distance-dependent model or using a non-distance-dependent model is small. Thus, we report both the geometric mean of the ratio of $Sa_{RotD100}$ and Sa_{RotD50} and the coefficient a_0 from equation 6 at different periods in table 1. Either of the two models can be used depending on the level of precision required. This view is echoed in the similar earlier study by Watson-Lamprey and Boore (2007), who noted slight distance, magnitude and radiation pattern dependence, but stated that "for most engineering applications the conversion factors independent of those variables can be used."

ORIENTATION OF $Sa_{RotD100}$

For most types of structures, the orientation in which the maximum spectral acceleration occurs is important. We define α as the minimum angle between the strike of the fault and the orientation of $Sa_{RotD100}$. This angle ranges from 0 to 90 degrees, where $\alpha = 0$ represents the strike-parallel orientation and $\alpha = 90$ represent the strike-normal orientation.

To study these orientations, we computed α for each ground motion at 21 periods, and then binned the data according to seismological parameters like magnitude, distance, directivity parameters and examined the distribution of α in each bin. Figure 3a shows the distribution of α observed in ground motions binned by magnitude (M) and closest distance (R_{rup}), and shows that α is closer to the strike-normal orientation ($\alpha = 90$) more often than to the strike-parallel orientation ($\alpha = 0$) when the recording is located within 5 km of the fault. On the other hand, when R_{rup} is greater than 5 km, α is almost uniformly distributed. The magnitude bins do not seem to have any significant influence on the distribution of α. To examine the effect of period on α, we binned all the data within 5 km of the fault by period as shown in figure 3b. The distribution of α is nearly uniform for periods less than 0.5 sec, while orientations close to strike-normal are more frequent than strike-parallel for periods larger than 0.5 sec (i.e., 1 sec and above). Five-degree bins were used to plot the density histograms shown in figure 3. Note that some judgment is required to infer the above-mentioned boundaries between uniform and non-uniform distributions of α in figure 3. Different observers may arrive at slightly different boundaries, but the general patterns are clear.

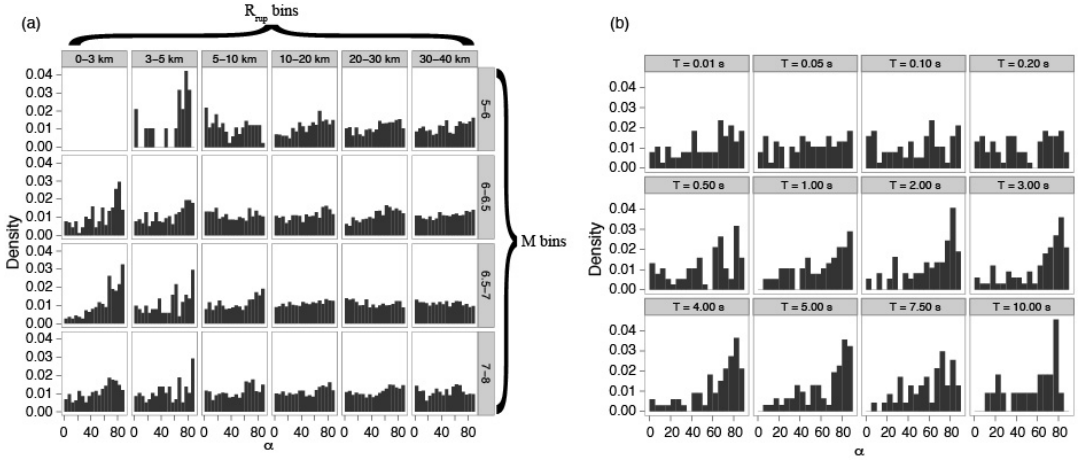

Figure 3. Probability density of α ($Sa_{RotD100}$ orientations), (a) binned by magnitude and closest distance, (b) binned by period (only for sites with $R_{rup} < 5$ km).

Figure 3, along with other similar figures showing no trends with other parameters (documented in Shahi and Baker, 2013) suggest that α is uniformly distributed when $R_{rup} > 5$ km or when $T < 1$ second. For other cases ($R_{rup} < 5$ km and $T \geq 1$ sec) the data was pooled and the distribution was modeled empirically by counting the fraction of motions with α observed in a given 10-degree bin. This empirical distribution is presented in table 2.

Table 2. Probability distribution of α for $R_{rup} < 5$km and $T \geq 1$ sec.

α orientation (degrees)	Probability
0-10	0.031
10-20	0.055
20-30	0.070
30-40	0.067
40-50	0.080
50-60	0.100
60-70	0.106
70-80	0.233
80-90	0.258

RELATIONSHIP BETWEEN $Sa_{RotD100}$ ORIENTATIONS AT DIFFERENT PERIODS

Figure 4 shows the polarization of displacement response and orientation of $Sa_{RotD100}$ intensity from an example ground motion at two different periods (say T^* and T'). The $Sa_{RotD100}$ intensity at different periods may occur in different orientations and the difference in orientation ($|\alpha^* - \alpha'|$ in figure 4) can be used to study the relationship between the $Sa_{RotD100}$ orientations at different periods. This knowledge can be used to construct more realistic single orientation target spectra, as shown below.

The difference in the orientation of $Sa_{RotD100}$ at two periods has a lot of uncertainty and can take any value between 0 degrees (i.e., the orientation at both period is the same) to 90 degrees (i.e., the $Sa_{RotD100}$ occurs in orthogonal orientations at the two periods). Figure 5 shows the histogram of the difference in $Sa_{RotD100}$ orientation ($|\alpha^* - \alpha'|$) at two different periods. The probability distribution of $|\alpha^* - \alpha'|$ depends on the periods under consideration, and the average difference between the orientations ($|\alpha^* - \alpha'|$) increases with increasing difference between the periods.

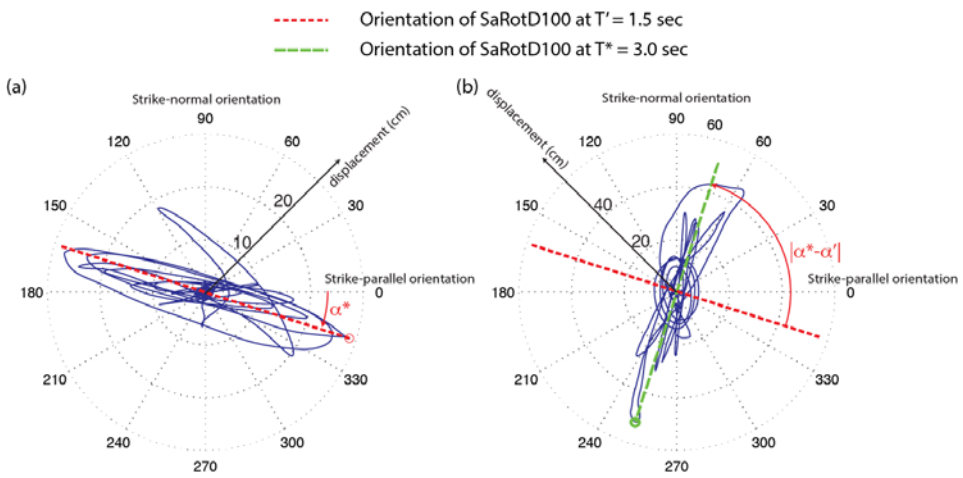

Figure 4. Displacement response trace of a single-degree-of freedom oscillator to the El Centro Differential Array recording from the 1979 Imperial Valley earthquake. The period of the single degree of freedom oscillator is (a) T^* = 1.5 sec and (b) T' = 3 sec. The orientations of $Sa_{RotD100}$ along with the difference between these orientations at the two periods ($|\alpha^* - \alpha'|$) is also shown.

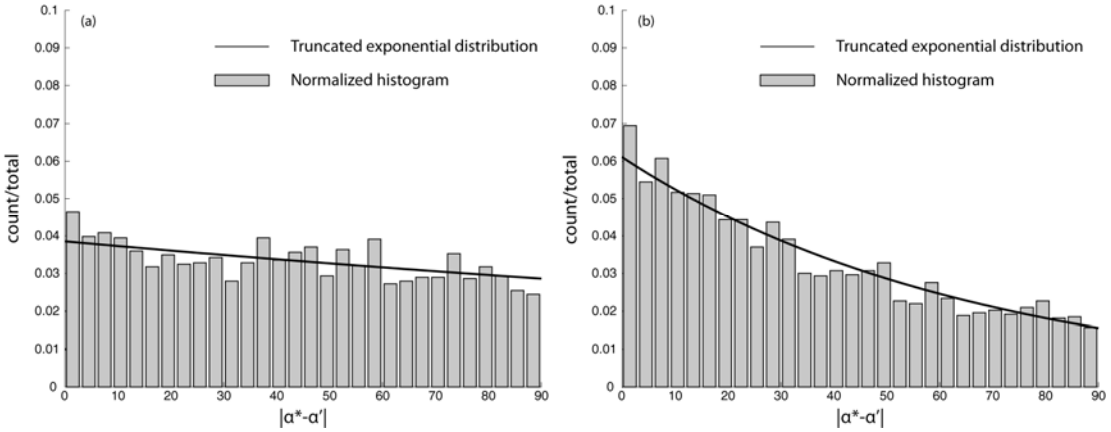

Figure 5. Distribution of $|\alpha^* - \alpha'|$ as predicted by the truncated exponential model is compared with the normalized histogram for (a) T^* = 2 sec and T' = 0.1 sec and (b) T^* = 2 sec and T' = 1 sec.

After examining histograms at several sets of periods, the truncated exponential distribution was selected to model the distribution of $|\alpha^* - \alpha'|$, as defined by the following probability density function

$$f(|\alpha^* - \alpha'|) = \begin{cases} \frac{\lambda e^{-\lambda|\alpha^* - \alpha'|}}{1 - e^{-90\lambda}}; & |\alpha^* - \alpha'| \leq 90 \\ 0; & otherwise \end{cases} \quad (7)$$

The distribution depends on the parameter λ, which is estimated here using the maximum likelihood method. The estimated parameters are presented in Table A1. When $T^* = T'$, $\lambda \to \infty$, and the probability density becomes a dirac-delta function centered at 0 degrees.

Figure 5 shows the comparison of the fitted distribution with empirical histograms for two periods.

Sa AT ARBITRARY ORIENTATIONS

The above models are not sufficient to predict *Sa* in an arbitrary orientation. Here we study the *Sa* in an orientation ϕ degrees away from the $Sa_{RotD100}$ orientation. This *Sa* is referred hereafter as Sa_{ϕ}. An empirical model for the ratio of Sa_{ϕ}/Sa_{RotD50} is developed, which can be used as a multiplicative factor with a ground-motion model prediction of Sa_{RotD50} to get a prediction for Sa_{ϕ}. As the event terms from mixed effect regression for $ln\,(Sa_{RotD100}/Sa_{RotD50})$ were found to be close to 0 above, we ignored the between-event terms and pooled the data across different earthquakes to empirically estimate the geometric mean of Sa_{ϕ}/Sa_{RotD50}. The $Sa_{RotD100}/Sa_{RotD50}$ values estimated using mixed effects regression (table 1), and empirical geometric means of the pooled data (values corresponding to $\phi = 0$ in table A2) vary slightly but are practically identical.

Table A2 shows the modeled ratios for different periods. The ratio is highest at $\phi = 0$, where it is same as $Sa_{RotD100}/Sa_{RotD50}$, and decreases with increasing ϕ. Table A2 presents the geometric mean of Sa_{ϕ}/Sa_{RotD50} for ϕ values in 10 degree intervals for 21 periods (results at 5 degree intervals are available in Shahi and Baker, 2013). Predictions at intermediate periods and ϕ values can be found by interpolating these results.

EXAMPLE TARGET SPECTRA

As discussed above, the $Sa_{RotD100}$ spectrum is an envelope over spectra from all orientations at each period. Figure 4 illustrates that even for two similar periods, the corresponding $Sa_{RotD100}$ values may be observed in very different orientations. It is very unlikely to observe $Sa_{RotD100}$ at multiple periods in a single orientation, so treating a $Sa_{RotD100}$ spectrum as the response spectrum of a single component of ground motion may result in conservative estimates of engineering demand parameters that are sensitive to excitations at multiple periods in a single direction (e.g., peak floor acceleration, inter-storey drift ratio etc.).

Conditional mean spectra approach (e.g., Baker, 2011) can be used to compute more realistic single orientation target spectra for design. The conditional mean spectrum is the

expected value of the ground-motion intensity conditioned upon some parameter values. Here we study the computation of two such target spectra conditioned on a specific orientation and on a $Sa_{RotD100}$ observation at a specific period.

SPECTRA CONDITIONED ON ORIENTATION

Structures generally have different load resistance in different orientations. If some orientation is more important than other orientations then the expected value of *Sa* in that particular orientation can be used as an appropriate target spectrum. Since this response spectrum is conditioned on a single orientation it does not suffer from the problem of having *Sa* from different orientations at different periods, as in case of the $Sa_{RotD100}$ spectra.

The target spectrum conditioned on an orientation, θ degrees away from strike-parallel orientation can be computed using the equation below

$$\begin{aligned} E[\ln Sa \mid \theta] &= \int_0^{90} E[\ln Sa_\theta \mid \alpha] \cdot P(\alpha)\, d\alpha \\ &= \int_0^{90} E[\ln Sa_{\theta-\alpha}] \cdot P(\alpha)\, d\alpha \\ &= \int_0^{90} \left(\ln\left(\frac{Sa_{\theta-\alpha}}{Sa_{RotD50}} \right) + \ln \hat{S}a_{RotD50} \right) \cdot P(\alpha)\, d\alpha \\ &= \ln \hat{S}a_{RotD50} + \int_0^{90} \ln\left(\frac{Sa_{\theta-\alpha}}{Sa_{RotD50}} \right) \cdot P(\alpha)\, d\alpha \end{aligned} \tag{8}$$

where α represents the orientation in which the $Sa_{RotD100}$ is observed at the period for which computation is being done and $\widehat{Sa}_{RotD50}$ represents the Sa_{RotD50} prediction from a ground-motion model. Table A2 gives the values of $Sa_{\theta-\alpha}/Sa_{RotD50}$ at different periods and $\phi = \theta - \alpha$ orientations. While table 2 describes the probability distribution of α (i.e. $P(\alpha)$).

Spectra conditioned in the strike-normal and strike-parallel orientations are compared with corresponding Sa_{RotD50} and $Sa_{RotD100}$ in figure 6a. The distance independent model (equation 5) was used to compute $Sa_{RotD100}$. These computations were done for an earthquake of magnitude 7 and at a site with V_{S30} of 760m/s and located 2.5 km away from the rupture. The Boore and Atkinson (2008) model was used to predict $Sa_{GMRotI50}$ and factors proposed in Boore (2010) were used to convert the $Sa_{GMRotI50}$ to Sa_{RotD50} prediction.

SPECTRA CONDITIONED ON THE ORIENTATION OF $Sa_{RotD100}$ AT A GIVEN PERIOD

Since, the orientation of $Sa_{RotD100}$ is random, the spectrum conditioned on a single orientation can never be as large as $Sa_{RotD100}$ at any period. Structural response is often primarily driven by the ground-motion intensity at a single period. Thus, if a single period is more important than others, a more appropriate target spectrum could be the one conditioned on the orientation in which $Sa_{RotD100}$ is observed at the important period (say T^*). If the spectrum is conditioned on $Sa_{RotD100}$ orientation at the period T^* (i.e., orientation = α^*) the expected value of the *Sa* at a different period, say T', can be computed using the equations below

$$\begin{aligned} E[\ln SaT' \mid \alpha^*] &= \int_0^{90} E[\ln SaT' \mid \alpha', \alpha^*] P(\alpha' \mid \alpha^*)\, d\alpha' \\ &= \int_0^{90} E[\ln SaT'_{|\alpha^* - \alpha'|} \mid \alpha', \alpha^*] P(|\alpha' - \alpha^*|)\, d\alpha' \\ &= \int_0^{90} \left(\ln\left(\frac{Sa_{|\alpha^* - \alpha'|}}{Sa_{RotD50}} \right) + \ln \hat{S}a_{RotD50} \right) P(|\alpha' - \alpha^*|)\, d\alpha' \\ &= \ln \hat{S}a_{RotD50} + \int_0^{90} \ln\left(\frac{Sa_{|\alpha^* - \alpha'|}}{Sa_{RotD50}} \right) P(|\alpha' - \alpha^*|)\, d\alpha' \end{aligned} \quad (4)$$

where $\frac{Sa_{|\alpha^* - \alpha'|}}{Sa_{RotD50}}$ is given by Table A2 for different values of $\phi = |\alpha^* - \alpha'|$ and periods (T'). $\widehat{Sa}_{RotD50}$ is the prediction from a ground-motion model and $P(|\alpha' - \alpha^*|)$ is modeled by the truncated exponential distribution from equation 7 with the parameter λ for the pair of periods T' and T^* given in table A1.

Spectra conditioned on the $Sa_{RotD100}$ orientations at T^* = 0.2 sec and T^* = 1 sec are compared with the Sa_{RotD50} and $Sa_{RotD100}$ in figure 6b. These computations were done for an earthquake of magnitude 7 and at a site with V_{S30} of 760m/s and located 2.5 km away from the rupture. Again the Boore and Atkinson (2008) model prediction and Boore (2010) conversion factors were used to estimate Sa_{RotD50}.

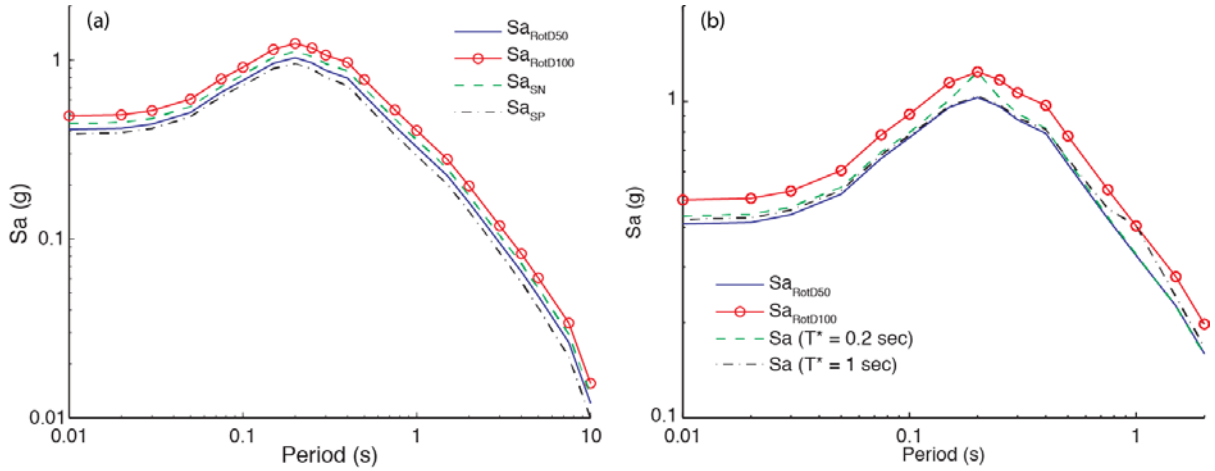

Figure 6. Comparison of the $Sa_{RotD100}$ and Sa_{RotD50} spectra with a) spectra conditioned in strike-normal (SN) and strike-parallel (SP) orientations, and b) spectra conditioned on $Sa_{RotD100}$ orientation at T^* = 0.2 sec and T^* = 1 sec. All results are for an earthquake with magnitude 7, at distance of 2.5 km and V_{S30} = 760 m/s.

CONCLUSIONS

In this study, we examined different methods of representing the intensity of ground motion in the horizontal plane using a response spectrum. We focused on two orientation-independent representations of the response spectrum: Sa_{RotD50} and $Sa_{RotD100}$. The ground-motion models developed as part of the NGA-West2 project predict the Sa_{RotD50} spectrum at a site due to a future earthquake, while some engineering provisions use $Sa_{RotD100}$ for design. We have computed the ratio of $Sa_{RotD100}$ to Sa_{RotD50}observed in recorded ground motions, which can be used as a multiplicative factor with Sa_{RotD50} predictions to predict the $Sa_{RotD100}$ ground-motion intensity. The computed ratios were compared, and found to be consistent with, similar models built in the past, though the results presented here advance that earlier work by using a larger data set, utilizing the recently adopted Sa_{RotD50} definition instead of $Sa_{GMRotI50}$ and using mixed effects regression to account for inter-event terms. The differences between the proposed model and corresponding NEHRP (2009) ratios were also explained. One important observation from this work is that the current NEHRP ratio of 1.1 at small periods is incorrect and should be approximately 1.2; this result is confirmed by other studies.

We also modeled the probability distribution of orientations in which the $Sa_{RotD100}$ intensity is observed relative to the strike of the fault. The orientations of $Sa_{RotD100}$ were observed to be uniformly distributed when the closest distance between the fault and the site was greater than 5 km or if the period under consideration was less than 0.5 sec. Only for the

cases when the site was within 5 km of the fault and at periods greater than 0.5 sec, the orientation of $Sa_{RotD100}$ was more likely to be closer to the strike-normal than strike-parallel direction. The relationship between the orientations of $Sa_{RotD100}$ at different periods was also studied and the difference between the orientations was modeled using a truncated exponential distribution. Together, these models can help solve a practical problem of converting between two important *Sa* definitions while helping deepen the understanding of the orientations in which $Sa_{RotD100}$ occurs and dependence of the $Sa_{RotD100}$ to Sa_{RotD50} ratio on various seismological parameters. Spectral predictions conditioned on a given orientation, or on the orientation in which $Sa_{RotD100}$ is observed at a particular period, were discussed. Example computations of these spectra using the models developed in the study were also presented. It should be noted that the models proposed in this study were developed to modify the Sa_{RotD50} predictions of ground-motion models. So care should be taken if users want to use these results to modify the final results of PSHA from Sa_{RotD50} to $Sa_{RotD100}$.

It is anticipated that these results will help bridge the gap between the works of seismic hazard analysts, who typically use Sa_{GM} or Sa_{RotD50} values, and design engineers, some of whom prefer to work with $Sa_{RotD100}$ response spectra.

ACKNOWLEDGEMENTS

This study was sponsored by the Pacific Earthquake Engineering Research Center (PEER) and funded by the California Earthquake Authority, California Department of Transportation, and the Pacific Gas & Electric Company. Any opinions, findings, and conclusions or recommendations expressed in this material are those of the authors and do not necessarily reflect those of the above-mentioned agencies. We thank the NGA-West2 Directionality Working group, consisting of Brian Chiou, Nico Luco, Mahmoud Hachem, Badie Rowshandel, Tom Shantz, Paul Spudich, and Jonathan Stewart for their helpful feedback and suggestions for this work. We also thank Yousef Bozorgnia and Carola Di Alessandro for their feedback, and Silvia Mazzoni, Damian Grant, Fabian Bonilla, and an anonymous reviewer for helpful review comments.

REFERENCES

Abrahamson, N., and Youngs, R. R., 1992. A stable algorithm for regression analysis using the random effects model. *Bulletin of the Seismological Society of America* 82(1), 505-510.

Abrahamson, N., 1998. Statistical properties of peak ground accelerations recorded by the SMART 1 array. *Bulletin of the Seismological Society of America* 78(1), 26-41.

Abrahamson, N., Atkinson, G., Boore, D., Bozorgnia, Y., Campbell, K., Chiou, B., Idriss, I. M., Silva, W., and Youngs, R., 2008. Comparisons of the NGA Ground-Motion relations. *Earthquake Spectra* 24 (1), 45-66.

Abrahamson, N., Silva, W.J., and Kamai, R., 2013. *Update of the AS08 Ground-Motion Prediction Equations Based on the NGA-West2 Data Set*. Technical report number 2013/04, Pacific Earthquake Engineering Research Center, Berkeley, California.

Al Atik, L., Abrahamson, N., Bommer, J. J., Scherbaum, F., Cotton, F., and Kuehn, N., 2010. The variability of ground-motion prediction models and its components. *Seismological Research Letters* 81 (5), 794-801.

Baker, J. W., 2011. The conditional mean spectrum: a tool for ground motion selection. *Journal of Structural Engineering* 137(3), 322-331.

Baker, J. W. and Cornell, C. A., 2006. Which spectral acceleration are you using? *Earthquake Spectra* 22 (2), 293-312.

Beyer, K. and Bommer, J. J., 2006. Relationships between median values and between aleatory variabilities for different definitions of the horizontal component of motion. *Bulletin of the Seismological Society of America* 96 (4A), 1512-1522.

Boore, D. M., 2010. Orientation-independent, nongeometric-mean measures of seismic intensity from two horizontal components of motion. *Bulletin of the Seismological Society of America* 100 (4), 1830-1835.

Boore, D. M. and Atkinson, G. M., 2008. Ground-Motion prediction equations for the average horizontal component of PGA, PGV, and 5%-Damped PSA at spectral periods between 0.01 s and 10.0 s. *Earthquake Spectra* 24 (1), 99-138.

Boore, D. M., Watson-Lamprey, J., and Abrahamson, N. A., 2006. Orientation-Independent measures of ground motion. *Bulletin of the Seismological Society of America* 96 (4A), 1502-1511.

Bozorgnia, Y., Abrahamson, N., Campbell, K., Rowshandel, B., and Shantz, T., 2012. NGA-West2: A comprehensive research program to update ground motion prediction equations for shallow crustal earthquakes in active tectonic regions. In *15th World Conference on Earthquake Engineering*, Lisbon, Portugal, 6pp.

Brillinger, D. R., and Preisler, H. K., 1985. Further analysis of the Joyner-Boore attenuation data. *Bulletin of the Seismological Society of America* 75(2), 611-614.

Campbell, K. W., and Bozorgnia, Y., 2007. *Campbell-Bozorgnia NGA ground motion relations for the geometric mean horizontal component of peak and spectral ground motion parameters*. Technical report number 2007/02, Pacific Earthquake Engineering Research Center, Berkeley, California. 238 pp.

Campbell, K. W., and Bozorgnia, Y., 2008. NGA ground motion model for the geometric mean horizontal component of PGA, PGV, PGD and 5% damped linear elastic response spectra for periods ranging from 0.01 to 10 s. *Earthquake Spectra* 24 (1), 139-171.

Chiou, B., Darragh, R., Gregor, N., and Silva, W., 2008. NGA project strong-motion database. *Earthquake Spectra* 24 (1), 23-44.

Hastie, T., Tibshirani, R., and Friedman, J. H., 2001. *The elements of statistical learning: data mining, inference, and prediction***.** New York: Springer.

Hong, H. P., and Goda, K., 2010. Characteristics of horizontal ground motion measures along principal directions. *Earthquake Engineering and Engineering Vibration*, *9*(1), 9-22.

Huang, Y., Whittaker, A., and Luco, N., 2010. *Maximum spectral demand in the United States*, USGS open file report xxx-xxxx. 217 pp.

Huang, Y., Whittaker A., and Luco, N., 2008. Maximum spectral demands in the Near-Fault region. *Earthquake Spectra* 24 (1), 319-341.

Jayaram, N., and Baker, J. W., 2008. Statistical tests of the joint distribution of spectral acceleration values. *Bulletin of the Seismological Society of America* 98(5), 2231-2243.

Kubo, T., and Penzien, J., 1976. Time and frequency domain analyses of three dimensional ground motions San Fernando earthquakes. Report of Engineering Earthquake Research Center, EERC 76-6, University of California, Berkeley, CA.

Kubo, T., and Penzien, J., 1979. Analysis of three-dimensional strong ground motions along principal axes, San Fernando earthquake. *Earthquake Engineering & Structural Dynamics*, *7*(3), 265-278.

Loh, C. H., Penzien, J., and Tsai, Y. B., 1982. Engineering analyses of SMART 1 array accelerograms. *Earthquake Engineering & Structural Dynamics*, *10*(4), 575-591.

Lopez, O. A., & Torres, R., 1997. The critical angle of seismic incidence and the maximum structural response. *Earthquake engineering & structural dynamics*, *26*(9), 881-894.

Lopez, O. A., Chopra, A. K., and Hernandez, J. J., 2000. Critical response of structures to multicomponent earthquake excitation. *Earthquake engineering & structural dynamics*, *29*(12), 1759-1778.

National Earthquake Hazard Reduction Program (NEHRP), 2009. *NEHRP Recommended Provisions for Seismic Regulations for New Buildings and Other Structures*. FEMA P-750. Federal Emergency Management Agency, Washington D.C.

Searle, S., 1971. *Linear Models*, John Wiley and Sons, Inc., New York, 560pp.

Shahi, S. K., and Baker, J. W., 2013. *NGA-West 2 models for ground-motion directionality*. Technical report number 2013/10, Pacific Earthquake Engineering Research Center, Berkeley, California.

Somerville, P.G., Smith, N. F., Graves, R. W., and Abrahamson, N. A., 1997. Modification of empirical strong ground-motion attenuation relations to include the amplitude and duration effects of rupture directivity. *Seismological Research Letters ,*68 (1), 199-222.

Spudich, P., Watson-Lamprey, J., Somerville, P., Bayless, J., Shahi, S. K., Baker, J. W., Rowshandel, B., and Chiou, B., 2012. Directivity models produced for the Next Generation Attenuation West 2 (NGA-West 2) project. In *15th World Conference on Earthquake Engineering*, Lisbon, Portugal, 9pp.

Stewart, J. P., Abrahamson, N. A., Atkinson, G. M., Baker, J., Boore, D. M., Bozorgnia, Y., Campbell, K.W., Comartin, C. D., Idriss, I. M., Lew, M., Mehrain, M., Moehle, J. P., Naeim, F., and Sabol, T. A., 2011. Representation of Bi-Directional Ground Motions for Design Spectra in Building Codes. *Earthquake Spectra*, 27(3), 927-937.

Watson-Lamprey, J., and Boore, D. M., 2007. Beyond SaGMRotI: conversion to SaArb, SaSN, and SaMaxRot. *Bulletin of the Seismological Society of America* 97 (5), 1511-1524.

APPENDIX

Table A1. Estimated values of the parameter λ for the truncated exponential model of equation 7. The table is symmetric, so only half of the coefficients are shown.

		T^*																			
		0.01	***0.02***	***0.03***	***0.05***	***0.07***	***0.10***	***0.15***	***0.20***	***0.25***	***0.30***	***0.40***	***0.50***	***0.70***	***1.00***	***1.50***	***2.00***	***3.00***	***4.00***	***5.00***	***7.50***	***10.0***
	0.01	∞																			
	0.02	0.579	∞																		
	0.03	*0.186*	*0.188*	∞																	
	0.05	0.070	0.071	0.072	∞																
	0.07	0.042	0.042	0.042	0.041	∞															
	0.10	0.031	0.031	0.030	0.028	0.031	∞											*sym.*			
	0.15	0.022	0.022	0.022	0.020	0.019	0.020	∞													
	0.20	0.021	0.021	0.021	0.019	0.017	0.015	0.019	∞												
	0.25	0.020	0.019	0.019	0.17	0.016	0.014	0.013	0.021	∞											
	0.30	0.020	0.020	0.019	0.017	0.016	0.014	0.013	0.016	0.026	∞										
T'	**0.40**	0.020	0.020	0.020	0.016	0.015	0.011	0.010	0.013	0.015	0.019	∞									
	0.50	0.018	0.018	0.018	0.015	0.013	0.011	0.009	0.011	0.010	0.013	0.024	∞								
	0.75	0.014	0.014	0.013	0.012	0.010	0.009	0.006	0.007	0.007	0.007	0.011	0.016	∞							
	1.00	0.013	0.013	0.012	0.010	0.009	0.007	0.005	0.005	0.005	0.007	0.010	0.013	0.022	∞						
	1.50	0.010	0.010	0.009	0.007	0.007	0.005	0.003	0.003	0.004	0.005	0.008	0.008	0.013	0.020	∞					
	2.00	0.007	0.007	0.007	0.006	0.005	0.003	0.002	0.003	0.004	0.003	0.005	0.007	0.011	0.015	0.024	∞				
	3.00	0.004	0.004	0.004	0.004	0.003	0.003	0.000	0.001	0.003	0.004	0.004	0.004	0.006	0.010	0.012	0.019	∞			
	4.00	0.005	0.005	0.006	0.005	0.004	0.003	0.001	0.002	0.003	0.004	0.006	0.005	0.008	0.010	0.011	0.016	0.029	∞		
	5.00	0.007	0.007	0.007	0.005	0.004	0.003	0.002	0.003	0.003	0.005	0.007	0.005	0.009	0.010	0.012	0.015	0.024	0.040	∞	
	7.50	0.007	0.007	0.007	0.006	0.004	0.003	0.002	0.002	0.003	0.004	0.005	0.005	0.009	0.011	0.013	0.016	0.019	0.025	0.034	∞
	10.0	0.007	0.007	0.007	0.005	0.005	0.003	0.002	0.002	0.003	0.005	0.005	0.005	0.009	0.010	0.013	0.014	0.017	0.021	0.027	0.057	∞

Table A2. Geometric mean of Sa_{ϕ}/Sa_{RotD50} at various values of ϕ and T.

		$\phi(degrees)$									
		0	**10**	**20**	**30**	**40**	**50**	**60**	**70**	**80**	**90**
	0.01	1.192	1.175	1.127	1.061	0.993	0.939	0.903	0.882	0.869	0.864
	0.02	1.191	1.174	1.127	1.061	0.993	0.939	0.904	0.882	0.869	0.865
	0.03	1.188	1.171	1.124	1.059	0.992	0.940	0.906	0.884	0.872	0.867
	0.05	1.187	1.170	1.123	1.058	0.992	0.941	0.908	0.877	0.874	0.870
	0.07	1.187	1.170	1.123	1.058	0.992	0.942	0.908	0.877	0.874	0.870
	0.10	1.186	1.168	1.122	1.058	0.993	0.941	0.906	0.882	0.868	0.864
	0.15	1.196	1.179	1.133	1.067	0.998	0.939	0.895	0.867	0.851	0.845
	0.20	1.204	1.187	1.140	1.074	1.003	0.938	0.887	0.854	0.835	0.829
	0.25	1.213	1.196	1.149	1.082	1.006	0.935	0.879	0.841	0.819	0.812
	0.30	1.217	1.200	1.153	1.084	1.008	0.935	0.874	0.830	0.803	0.794
T'	**0.40**	1.227	1.209	1.162	1.093	1.013	0.934	0.868	0.819	0.789	0.779
	0.50	1.228	1.210	1.163	1.094	1.013	0.933	0.863	0.811	0.780	0.770
	0.75	1.236	1.219	1.171	1.100	1.017	0.933	0.857	0.798	0.761	0.749
	1.00	1.239	1.222	1.173	1.102	1.017	0.931	0.854	0.795	0.757	0.745
	1.50	1.236	1.219	1.171	1.100	1.016	0.932	0.855	0.795	0.757	0.744
	2.00	1.240	1.222	1.174	1.102	1.018	0.930	0.851	0.789	0.750	0.737
	3.00	1.247	1.229	1.180	1.108	1.021	0.929	0.845	0.778	0.734	0.719
	4.00	1.257	1.240	1.190	1.116	1.026	0.929	0.837	0.761	0.708	0.688
	5.00	1.264	1.246	1.196	1.121	1.029	0.928	0.828	0.740	0.677	0.652
	7.50	1.284	1.266	1.215	1.138	1.039	0.928	0.810	0.699	0.608	0.565
	10.00	1.290	1.272	1.221	1.141	1.041	0.927	0.806	0.688	0.589	0.542